Turbulence, Heat and Mass Transfer 8

Two-equation hybrid RANS-LES Models: A novel way to treat k and ω at the inlet

L. Davidson

Division of Fluid Dynamics, Department of Applied Mechanics, Chalmers University of Technology, SE-412 96 Gothenburg, Sweden, lada@chalmers.se

Abstract —

A novel method for prescribing inlet conditions for k and ω is presented and evaluated. The method is based on the proposal by Hamda [1] to use commutation terms at RANS-LES interfaces. Commutation terms are added in the region near the inlet (i.e. the RANS-LES interface) in the k and ω equations. It is found that it is preferable to add the commutation terms only in the cells adjacent to the inlet. The discretized commutation term in the k equation reads $P^{k,c} = \bar{u}_{in}(k_{LES} - k_{RANS})/\Delta x \simeq -\bar{u}_{in}k_{RANS}/\Delta x$ since k_{LES} is negligible. Hence, this term corresponds to a convection term where k is reduced from its RANS value to zero over one cell layer. The corresponding term in the ω equation reads $-P^{k,c}\omega_{RANS}/k_{RANS}$. In this way tuned constants are avoided.

Anisotropic synthetic fluctuations are used in the momentum equations as inlet conditions. The mean velocity, k, ω and the Reynolds shear stress profile are taken from a pre-cursor RANS simulation. The anisotropy of the synthetic fluctuations is defined from the EARSM model. No tuned constants are used.

1. Introduction

When using hybrid RANS-LES, instantaneous resolved, turbulent fluctuations must be given at the inlet. In the literature, they are usually created by synthetic turbulence generators (assuming that the turbulence obeys a Kolmogorov $-5/3$ spectrum) or synthetic eddy methods. If the hybrid RANS-LES model includes transport equations for modeled, turbulent quantities, the questions arises, how to prescribe inlet boundary conditions for these quantities? This is the issue of the present study. The method is validated in channel flow and flat-plate boundary layer flow.

2. The Zonal $k-\omega$ Hybrid RANS-LES Model

In the LES region the model reads

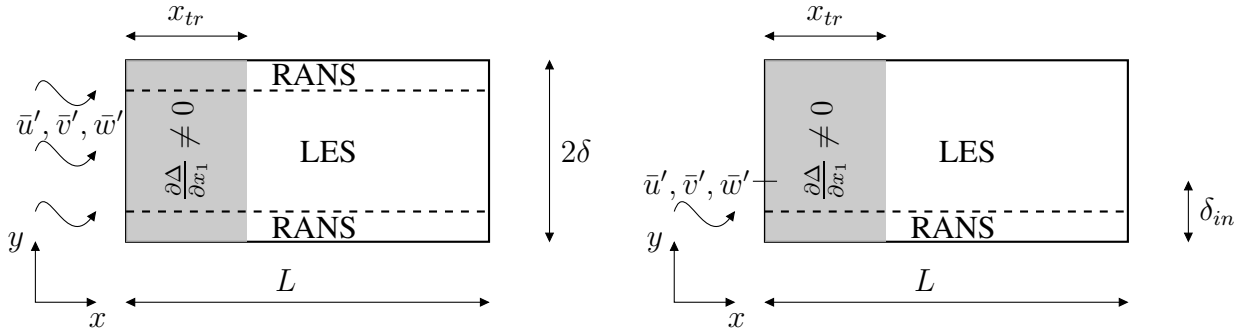

(a) Channel flow.

(b) Boundary layer flow.

Figure 1: Computational domains.

$$\frac{\partial k}{\partial t}+\frac{\partial \bar{v}_i k}{\partial x_i}=P^k-f_k\frac{k^{3/2}}{\ell_t}+\frac{\partial}{\partial x_j}\left[\left(\nu+\frac{\nu_t}{\sigma_k}\right)\frac{\partial k}{\partial x_j}\right] \tag{1}$$

$$\frac{\partial \omega}{\partial t}+\frac{\partial \bar{v}_i \omega}{\partial x_i}=C_{\omega_1}f_\omega\frac{\omega}{k}P^k-C_{\omega 2}\omega^2+\frac{\partial}{\partial x_j}\left[\left(\nu+\frac{\nu_t}{\sigma_\omega}\right)\frac{\partial \omega}{\partial x_j}\right]+C_\omega\frac{\nu_t}{k}\frac{\partial k}{\partial x_j}\frac{\partial \omega}{\partial x_j}$$

$$\nu_t=f_\mu\frac{k}{\omega},\quad P^k=\nu_t\left(\frac{\partial \bar{u}_i}{\partial x_j}+\frac{\partial \bar{u}_j}{\partial x_i}\right)\frac{\partial \bar{u}_i}{\partial x_j},\quad \ell_t=\Psi_{PDH}C_{LES}\Delta_{dw}$$

$$\Psi_{PDH}=\min\left[10,f_k\left(\frac{f_\omega}{f_\mu}\right)^{3/4}\right],\quad \Delta_{dw}=\min\left(\max\left[C_{dw}d_w,C_w\Delta_{max},\Delta_{nstep}\right],\Delta_{max}\right)$$

$$f_k=1-0.722\cdot\exp\left[-\left(\frac{R_t}{10}\right)^4\right],\quad f_\omega=1+4.3\cdot\exp\left[-\left(\frac{R_t}{1.5}\right)^{1/2}\right]$$

$$f_\mu=0.025+\left\{1-\exp\left[-\left(\frac{R_t}{10}\right)^{3/4}\right]\right\}\left\{0.975+\frac{0.001}{R_t}\cdot\exp\left[-\left(\frac{R_t}{200}\right)^2\right]\right\}$$

The turbulent Reynolds number is defined as $R_t=k/(\nu\omega)$. The length scale, Δ_{dw}, is taken from the IDDES model [2]. In the RANS regions, $\ell_t=k^{1/2}/(C_k\omega)$. The constants read $\sigma_k=0.8$, $\sigma_w=1.35$, $C_k=0.09$ $C_{\omega 1}=0.42$, $C_{\omega 2}=0.075$, $C_\omega=0.75$, $C_{LES}=0.7$, $C_{dw}=0.15$. Details on the zonal $k-\omega$ Hybrid RANS-LES Model can be found in [3, 4].

3. Numerical method

An incompressible, finite volume code is used [5]. The convective terms in the momentum equations are discretized using central differencing. Hybrid central/upwind is used for the k and ω equations. The Crank-Nicolson scheme is used for time discretization of all equations. The numerical procedure is based on an implicit, fractional step technique with a multigrid pressure Poisson solver [6] and a non-staggered grid arrangement.

4. Treatment of k and ω at the inlet

When the filter size in LES varies in space, an additional term appears in the momentum equation because the spatial derivatives and the filtering do not commute. For the convective term in Navier-Stokes, for example, we get

$$\overline{\frac{\partial v_i v_j}{\partial x_j}}=\frac{\partial}{\partial x_j}(\overline{v_i v_j})+\mathcal{O}\left((\Delta x)^2\right)$$

In [7] it was shown that the error is proportional to $(\Delta x)^2$, and since this error is of the same order as the discretization error of most finite volume methods, it is usually neglected.

However, in zonal[1] hybrid RANS-LES, the length scale at the RANS-LES interface changes abruptly from a RANS length scale to a LES length scale. Hamda [1] has estimated the commutation error at RANS-LES interfaces and he found that it is large. The commutation term for the divergence of a flux, q_i, reads

$$\overline{\frac{\partial q_i}{\partial x_i}}=\frac{\partial \bar{q}_i}{\partial x_i}-\frac{\partial \Delta}{\partial x_i}\frac{\partial \bar{q}_i}{\partial \Delta}$$

[1] by "zonal", we imply that the interface is chosen at a location where the RANS and LES length scales differ

For the k equation the commutation term reads [1]

$$\overline{\frac{\partial u_i k}{\partial x_i}} = \frac{\partial \bar{u}_i k}{\partial x_i} - \frac{\partial \Delta}{\partial x_i}\frac{\partial \bar{u}_i k}{\partial \Delta} \tag{2}$$

Consider a fluid particle in a RANS region moving in the x_1 direction and passing across a RANS-LES interface. The filterwidth decreases across the interface ($\partial\Delta/\partial x_1 < 0$) and $\partial \bar{u}_1 k/\partial\Delta = (k_{LES} - k_{RANS})/(\Delta_{LES} - \Delta_{RANS}) > 0$ which means that the second term in Eq. 2 gives a positive/negative contribution on the left-side/right-side of the k equation (Eq. 1). Hence, the additional term in Eq. 2 at a RANS-LES interface reduces k. It may be noted that the idea of adding an additional source term in the k equation due to a commutation error is similar to the proposal in [8]; here they use a commutation term based on the gradient of f_k in the PANS model. This idea was later used by the present author at RANS-LES interfaces [9].

In order to find the corresponding term in the ω equation, let us start by looking at the ε equation. What happens with ε when a fluid particle moves from a RANS region into an LES region? The answer is, nothing. The dissipation is the same in a RANS region as in an LES region. Now consider the ω equation. It is derived by transformation of the k and ε equations to an ω equation as

$$\frac{d\omega}{dt} = \frac{d}{dt}\left(\frac{\varepsilon}{C_k k}\right) = \frac{1}{C_k k}\frac{d\varepsilon}{dt} + \frac{\varepsilon}{C_k}\frac{d(1/k)}{dt} = \frac{1}{C_k k}\frac{d\varepsilon}{dt} - \frac{\omega}{k}\frac{dk}{dt} \tag{3}$$

The source terms in the ω equation correspond to those in the ε equation multiplied by $1/(C_k k)$ together with those in the k equation multiplied by $-\omega/k$. Hence, the source term due to the commutation error in the ω equation is the commutation term in Eq. 2 multiplied by $-\omega/k$ (see the second term in Eq. 3) so that

$$\overline{\frac{\partial u_i \omega}{\partial x_i}} = \frac{\partial \bar{u}_i \omega}{\partial x_i} - \frac{\partial \Delta}{\partial x_i}\frac{\partial \bar{u}_i \omega}{\partial \Delta} = \frac{\partial \bar{u}_i \omega}{\partial x_i} + \frac{\omega}{k}\frac{\partial \Delta}{\partial x_i}\frac{\partial \bar{u}_i k}{\partial \Delta} \tag{4}$$

This means that the commutation term in Eq. 4 will increase ω when moving from a RANS region to an LES region. Hence the source terms in the k and ω equations both contribute to reduce the turbulent viscosity which is an effect we are looking for at RANS-LES interfaces: a reduced turbulent viscosity will promote growth of resolved turbulence on the LES side of the interface. Inlet values for k and ω are taken from a pre-cursor RANS simulation.

The commutation terms in Eqs. 2 and 4 are added in the transition region, $0 < x < x_{tr}$ (see Fig. 1); for the k equation it is discretized as follows.

$$P^{k,c} = \frac{\partial \Delta}{\partial x_1}\frac{\partial \bar{u}_{in} k}{\partial \Delta}\bigg|_x = \left(\frac{\Delta_{LES} - \Delta_{RANS}}{x_{tr}}\right)\left(\frac{\bar{u}_{in} k_{RANS,x} - \bar{u}_{in} k_{LES}}{\Delta_{RANS} - \Delta_{LES}}\right) = \bar{u}_{in}\frac{k_{LES} - k_{RANS,x}}{x_{tr}}$$
$$k_{LES} = \left(\frac{\nu_{sgs}}{\Delta}\right)^2, \quad \nu_{sgs} = (C_s\Delta)^2\,|\bar{s}|, \quad \Delta = (\Delta V)^{1/3}, \quad C_s = 0.1 \tag{5}$$

where k_{LES} is evaluated in the cells near the outlet, i.e. in the LES region; evaluating k_{LES} in the cells adjacent to the inlet has negligible influence on the predictions (it is shown below that k_{LES} is negligible). Initially, k_{RANS} was evaluated at the inlet, but that gives too large a gradient and the simulations diverge. Instead, k_{RANS} is evaluated at the local x station (denoted by $k_{RANS,x}$) in the transition region. This ensures that the magnitude of the commutation term decreases smoothly from $x = 0$ to x_{tr}.

The commutation terms should formally only be applied in the LES region and not in the RANS regions near the walls. However, we know that the turbulent viscosity in fully-developed channel flow using hybrid LES-RANS models is much smaller than in pure RANS simulations (see, e.g., Fig. 8a in [10]). Hence we need to add commutation terms also in the RANS regions in order to reduce the turbulent viscosity. In the RANS regions, k_{LES} in Eq. 5 should be replaced with k_{URANS} where k_{URANS} denotes the modeled turbulence kinetic energy in the unsteady RANS region. But since it is not obvious how to define k_{URANS}, Eq. 5 is used also in the RANS regions.

5. Synthetic fluctuations

Anisotropic synthetic fluctuations are superimposed to the mean flow profiles at the inlet. The methodology used in [11, 12] is somewhat extended and involves the following steps.

1. A pre-cursor RANS simulation (1D for the channel flow and 2D for the boundary layer flow) is made using the PDH model [13].

2. The Reynolds stress tensor is computed using the EARSM model [14].

3. The Reynolds stress tensor is used as input for generating the anisotropic synthetic fluctuations.

4. Since the method of synthetic turbulence fluctuations assumes homogeneous turbulence, we can only use the Reynolds stress tensor in one point. We need to chose a relevant location for the Reynolds stress tensor. In boundary layer flow, the turbulent shear stress is the single most important stress component. Hence, the Reynolds stress tensor is taken at the location where the magnitude of the turbulent shear stress is largest.

5. Finally, the synthetic fluctuations are scaled with $\left(|\overline{u'v'}|/|\overline{u'v'}|_{max}\right)^{1/2}_{RANS}$ which is taken from the RANS simulation.

Figure 2 shows the prescribed synthetic fluctuations. The fluctuations differ slightly between the channel flow and the boundary flow because the Reynolds stress tensor from EARSM as well as the shear stress from the RANS solutions are slightly different.

Matlab files for generation of the anisotropic fluctuations can be found in [15].

6. Results

6.1. Channel flow

For the channel flow, the Reynolds number is $Re_\tau = 8\,000$. A $256 \times 96 \times 32$ mesh is used with $\Delta x = 0.1$, $\Delta z = 0.05$; a geometric stretching of 15% is used in the y direction ($y_{max} = 2 = 2\delta$). The mean inlet velocity profile is taken from a fully developed simulation using the Zonal $k-\omega$ Hybrid RANS-LES Model. The k and ω are taken from a 1D RANS solution using the PDH model. The wall-parallel RANS-LES interface is prescribed at a fixed gridline at $y^+ \simeq 500$.

Figures 3 presents the turbulent viscosities, the modeled turbulent kinetic energy and the friction velocity for different extensions of the transition region, x_{tr}. Figure 3a shows that the smaller x_{tr}, the more rapidly the turbulent viscosity is reduced. When $x_{tr}/\delta = 0.1$, the reduction takes place over one cell. In this case the commutation term is simply $P^{k,c} = \bar{u}(k_{LES} - k_{RANS})/\Delta x \simeq -\bar{u}k_{RANS}/\Delta x$ (see Eq. 5) since k_{LES} is negligible, see Fig. 3d (this explains why it is unimportant where k_{LES} is evaluated as mentioned below Eq. 5). Hence the

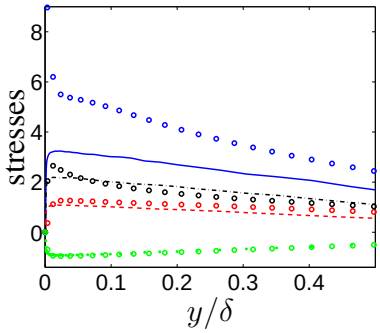

(a) Channel flow. Markers: DNS at $Re_\tau = 4\,200$ [16].

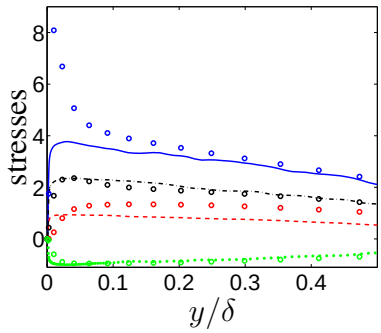

(b) Boundary layer flow. Markers: DNS at $Re_\theta = 8\,300$ [17].

Figure 2: Added synthetic Reynolds stresses at the inlet. —: $\langle u'u' \rangle^+$; - - -: $\langle v'v' \rangle^+$; -·-·-: $\langle w'w' \rangle^+$; ···: $\langle u'v' \rangle^+$.

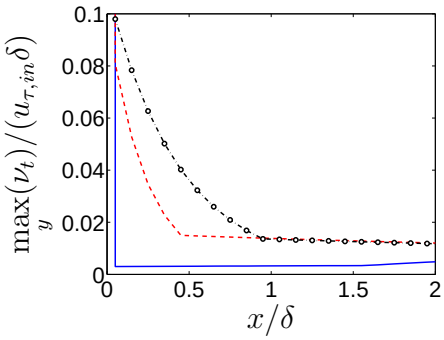

(a) Maximum turbulent viscosity in the LES region.

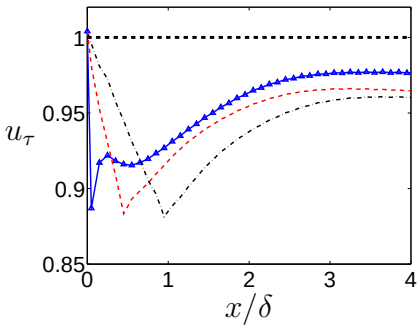

(b) Friction velocity. - - -: target value. Markers indicate location of cell centers.

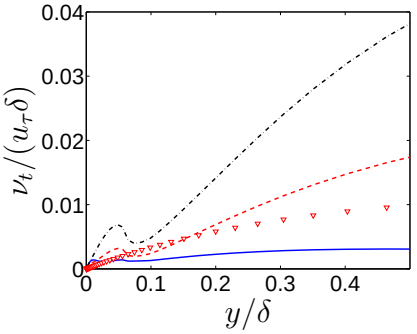

(c) Turbulent viscosity. $x/\delta = 0.25$. ▽: $\nu_t/10/(u_\tau\delta)$ at inlet (i.e. RANS).

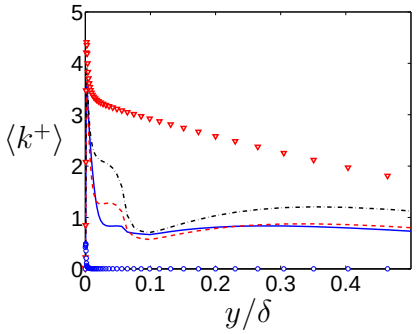

(d) Modeled turbulent kinetic energy. $x/\delta = 0.25$. ▽: $\langle k^+ \rangle$ at inlet (i.e. RANS); ○: k_{LES} for $x_{tr}/\delta = 0.1$, see Eq. 5.

Figure 3: Channel flow. —: $x_{tr}/\delta = 0.1$; - - -: $x_{tr}/\delta = 0.5$; -·-·-: $x_{tr}/\delta = 1$.

commutation term for $x_{tr}/\delta = 0.1$ corresponds to a convection term where k goes from its RANS (i.e. inlet) value to zero over one cell. The influence on the friction velocity (Fig. 3b) is similar as on the turbulent viscosities: the smaller the transition region, the earlier the minimum of u_τ is located. In fact, the minimum is located at the end of the transition region. As a consequence, the larger x_{tr}, the longer distance it takes for u_τ to reach its fully-developed flow value (close to one). The reason why the fully-developed value of u_τ is not one is that the synthetic fluctuations are not perfect: when inlet fluctuations are taken from a fully-developed channel

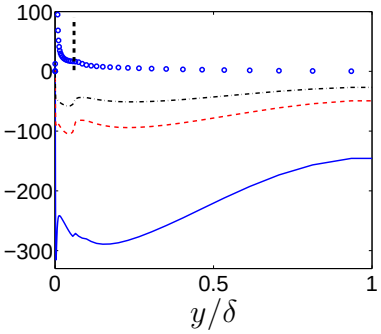

(a) $x/\delta = 0.05$. ○: Production term, P^k, $x_{tr} = 0$; ——: commutation term (Eq. 5), $x_{tr}/\delta = 0.1$; – – : commutation term, $x_{tr}/\delta = 0.5$; –·– : commutation term, $x_{tr}/\delta = 1$.

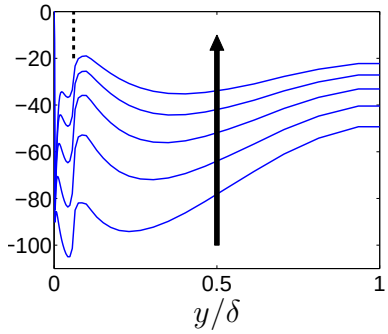

(b) Commutation term (Eq. 5) at different locations. $x_{tr}/\delta = 0.5$. $x/\delta = 0.05, \ldots 0.45$. The arrow indicates increasing x.

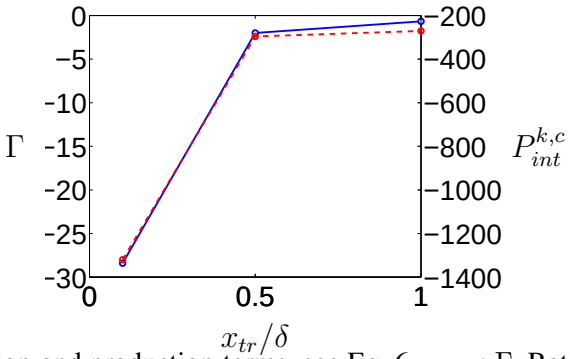

(c) Mean commutation and production terms, see Eq. 6. ——: Γ, Ratio of mean commutation term to production term (left axis); – – : $P^{k,c}_{int}$, mean production term (right axis).

Figure 4: Channel flow. Source terms in the k equation.

flow using the Zonal $k-\omega$ Hybrid RANS-LES Model, the friction value does indeed quickly go to one (not shown). Figures 3c and d confirm the findings above, namely that the shorter the transition region, the more quickly resolved turbulence is created and modeled turbulence reduced.

Figure 4 show the production and commutation term in the k equation close to the inlet. First, it should be noted that the magnitude of the commutation term is very large (Fig. 4a), much larger than the production term, but it decreases with increasing transition length. It also decreases with x, see Fig. 4b. Figure 4c presents the mean commutation term, $P^{k,c}_{int}$, over the entire transition region scaled with the mean production, P^k_{int}, i.e.

$$\Gamma = \frac{\frac{1}{x_{tr}\delta z_{max}} \int_0^{x_{tr}} \int_0^{\delta} \int_0^{z_{max}} P^{k,c} dx dy dz}{\frac{1}{x_{tr}\delta z_{max}} \int_0^{x_{tr}} \int_0^{\delta} \int_0^{z_{max}} P^{k} dx dy dz} = \frac{P^{k,c}_{int}}{P^{k}_{int}} \tag{6}$$

see Eq. 5. Note that $x_{tr}/\delta = 0.1$ means that the commutation terms in the k and ω equations are active only in one cell layer (adjacent to the inlet). It can be seen that for $x_{tr}/\delta = 0.1$, the magnitude of the mean commutation term in the k equation is more than 30 times larger than the mean production term. The ratio decreases fast when the transition region is enlarged (from 30 to one). The red, dashed line shows the mean commutation term, $P^{k,c}_{int}$. This term decreases much slower (by a factor of seven) than Γ which means that the production term increases for

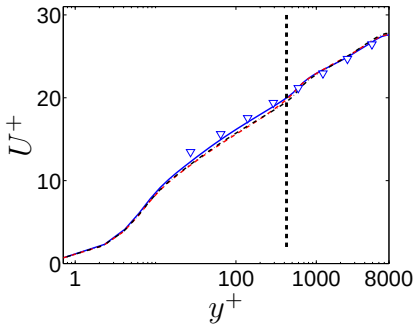

(a) Velocity. ——: inlet; – – –: $x = 2.5\delta$; –·–·–: $x = 24\delta$; ▽: $U^+ = \ln(y^+)/0.4 + 5.2$

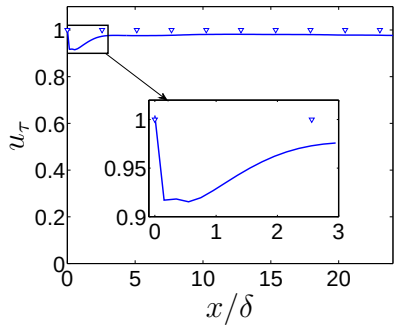

(b) Friction velocity. ▽: $u_\tau = 1$ (target value)

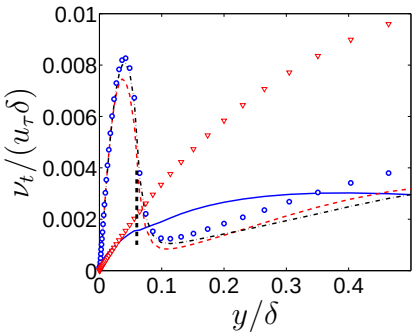

(c) Turbulent viscosity. ——: $x = 0.05\delta$; – – –: $x = 2.5\delta$; –·–·–: $x = 5.65\delta$; ▽: $\nu_t/(u_\tau\delta)/10$ at inlet (i.e. RANS).

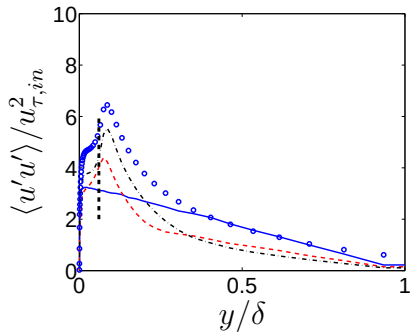

(d) Resolved turbulent stress. ——: $x/\delta = 0.05$; – – –: $x = 2.5\delta$; –·–·–: $x = 5.85\delta$.

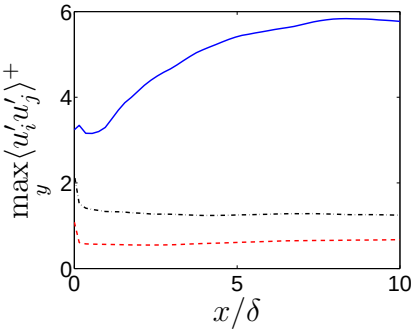

(e) Maximum resolved turbulent fluctuations. ——: $\langle u'u'\rangle^+$; – – –: $\langle v'v'\rangle^+$; –·–·–: $\langle w'w'\rangle^+$.

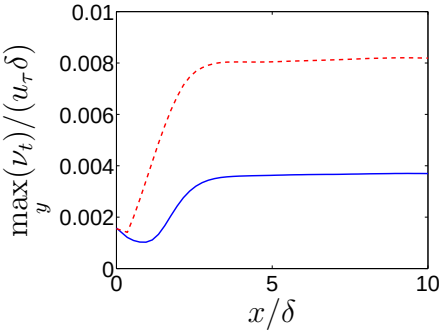

(f) Maximum turbulent viscosity. ——: LES region; – – –: RANS region.

Figure 5: Channel flow. ○: fully developed channel flow with Zonal hybrid RANS-LES model. Vertical thick dashed line indicates the RANS-LES interface.

increasing transition length; this leads to the reduced relative influence of the commutation term as the transition length is increased, illustrated by the decreasing Γ.

Above, $x_{tr}/\delta = 0.1$ was found to be the most efficient option for quickly creating resolved turbulence. Hence, below we use $x_{tr}/\delta = 0.1$ for analyzing the flow in more detail. Figure 5 show that the velocities and the friction velocity are well predicted. It takes less than 3δ for the friction velocity (Fig. 5b) to reach its fully-developed value. Figure 5c shows that the turbulent viscosity is reduced from its inlet value (i.e. RANS) down to values corresponding to fully-developed hybrid LES-RANS flow already at $x/\delta_{in} = 0.05$ (i.e. the cells adjacent to the inlet). Figure 5d presents the resolved turbulent streamwise fluctuations, and it can be seen that the resolved turbulence is quickly established although it takes rather long distance to reach values

close to fully-developed hybrid LES-RANS.

Figure 5e and f show the development of the peaks of resolved fluctuations and turbulent viscosity. It can be seen that fluctuations reach their fully-developed peaks after approximately eight half channel heights (the streamwise fluctuations develop much slower than the other two). The peak of the turbulent viscosity becomes fully developed at $x/\delta \simeq 3$.

As mentioned below Eq. 5, the commutation terms are used also in the RANS regions. It turns out that setting the commutation terms to zero in the RANS region has negligible effect on the results (not shown). The main difference is that the turbulent viscosity at $x/\delta = 0.05$ is much larger (the peak is approximately twice as large as in Fig. 5c).

6.2. Boundary layer flow

For the developing boundary layer flow, the Reynolds number is $Re_\theta = 11\,000$ ($Re_{\tau,in} = 3\,400$). A $128 \times 192 \times 32$ mesh is used with $\Delta x = 0.1$, $\Delta z = 0.05$; a geometric stretching of less than 15% is used in the boundary layer in the y direction. The inlet boundary layer thickness ($\delta_{in} = 0.8$) is covered by approximately 110 cells. The mean inlet velocity profile is taken from the linear and the log-law which are connected with another log law in the buffer layer

$$U^+_{in} = \begin{cases} y^+ & y^+ \leq 5 \\ -2.23 + 4.49\ln(y^+) & 5 < y^+ < 30 \\ \dfrac{1}{\kappa}\ln(y^+) + B + \dfrac{2\Pi}{\kappa}\sin^2\left(\dfrac{\pi y}{2\delta}\right) & y^+ \geq 30 \end{cases} \tag{7}$$

where $\kappa = 0.38$, $B = 4.1$ and $\Pi = 0.5$ [18, 19]. The k and ω are taken from a RANS solution using the PDH model. The reason the velocity is not taken from a RANS simulation is that the RANS predictions do not predict a proper relation between the skin friction and the momentum thickness (e.g. $C_f = 0.03Re_\theta^{-0.268}$ [20, Eq. 7-79]). The wall-parallel RANS-LES interface is prescribed at a fixed gridline at $y^+ \simeq 500$.

Figure 6 presents the sensitivity to the transition length for the boundary layer flow. Contrary to the channel flow (Fig. 3a), the turbulent viscosity is sufficiently reduced only with $x_{tr}/\delta_{in} = 0.125$. As a consequence, the skin friction in Fig.6b is accurately predicted only with $x_{tr}/\delta_{in} = 0.125$ whereas $x_{tr}/\delta_{in} = 0.25$ and 0.375 gives too small a skin friction. With $x_{tr}/\delta_{in} = 0.125$, an accurate value is obtained within two boundary layer thicknesses. The turbulent viscosity profiles in Fig. 6c show that the turbulent viscosity is strongly reduced at the cells adjacent to the inlet; the reduction in the LES region close to the RANS-LES interface compared to the inlet value is approximately 70 for $x_{tr}/\delta_{in} = 0.125$. For $x_{tr}/\delta_{in} = 0.25$ and 0.375, the turbulent viscosity is slightly affected near the RANS-LES interface, but it increases rapidly further out from the wall. It can be noted that the modeled turbulent kinetic energy, k (Fig. 6d), is influenced much less than the turbulent viscosity (Fig. 6c) by the transition length. This indicates that ω is fairly sensitive to x_{tr}. This is indeed the case as can be seen in Fig. 7. We see that the commutation term in Eq 4 increases ω also for $x_{tr}/\delta_{in} = 0.25$ and 0.375 (at least in the RANS region), but the increase is not sufficient to generate a substantial decrease in the turbulent viscosity. Figure 6d also include k_{LES} in the commutation term (see Eq. 5) which, as in the channel flow (cf. Fig. 3d) is negligible compare to k_{RANS}.

Figure 8 presents the production and the commutation terms in the k equation. As in the channel flow, the commutation term is much larger than the production term (Fig. 8a). It is as large as in the channel flow. The streamwise gradient of the commutation term, see Fig. 8b, is also as large as in the channel flow (cf. Fig. 4b). Also the integrated commutation term, see Fig. 8c (right axis), is as large as in the channel flow (cf. Fig. 4c, right axis); indeed, for larger

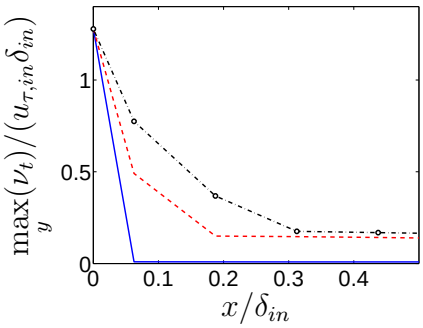

(a) Maximum turbulent viscosity in the LES region. Markers denote location of cell centers.

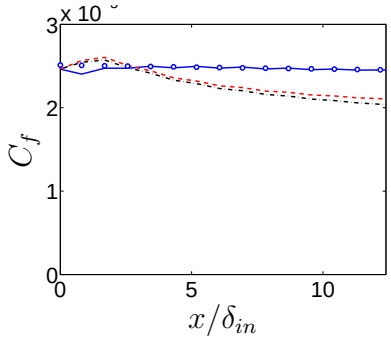

(b) Skin friction. ○: target value. Markers indicate location of cell centers.

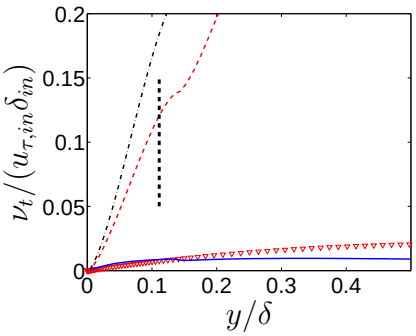

(c) Turbulent viscosity. $x/\delta_{in} = 0.06$. ▽: $\nu_t/(60u_{\tau,in}\delta_{in})$ at inlet (i.e. RANS).

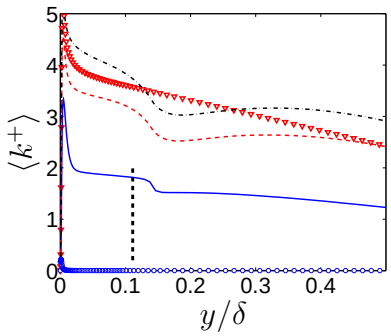

(d) Modeled turbulent kinetic energy. $x/\delta_{in} = 0.06$. ▽: at inlet (i.e. RANS); ○: k_{LES} for $x_{tr}/\delta = 0.1$, see Eq. 5.

Figure 6: Boundary layer flow. —: $x_{tr}/\delta = 0.125$; - -: $x_{tr}/\delta_{in} = 0.25$; -·-: $x_{tr}/\delta_{in} = 0.375$; ▽: at inlet (i.e. RANS). Vertical thick dashed line indicates the RANS-LES interface.

x_{tr} it is even larger than in the channel flow. However, the integrated ratio of the commutation term to the production term, see Fig. 8c (left axis), is much smaller than in the channel flow (cf. Fig. 4c, left axis). This is also seen when comparing the local production terms in Figs. 8a and 4a. Their peaks are similar, but the production term in the boundary layer is larger than in the channel flow further out from the wall. Hence, the reason for the smaller Γ in Fig. 8c compared to in Fig. 4c is the large integrated production term in the boundary layer flow. This explains why the commutation term in the boundary layer flow is efficient only for $x_{tr}/\delta_{in} = 0.125$.

Figure 9 shows that for $x_{tr}/\delta_{in} = 0.125$, the flow reaches fully developed conditions fairly rapidly: after approximately $5\delta_{in}$ the velocity profiles (Fig. 9a), the skin friction (Fig. 9b), the turbulent viscosities (Fig. 9c, f) and the resolved turbulence (Fig. 9d, e) have reached the fully-developed values. The resolved turbulence agrees well with DNS data already at $x_{tr}/\delta_{in} = 0.06$ (Fig. 9d) and the turbulent viscosity is reduced from the RANS (inlet) value at $y/\delta_{in} = 0.2$ by a factor of 80 (Fig. 9c).

It was mentioned above that, for channel flow, setting the commutation terms in the k and ω equations to zero in the RANS regions has negligible effects on the predicted results. However, Fig. 10 shows that for boundary-layer flow the effect is substantial. The skin friction (Fig. 10b) is much worse predicted with a peak near the inlet; further downstream is becomes too small. The turbulent viscosity (Fig. 10c) is much larger (cf. Fig. 9c) and as a consequence the resolved turbulence in the wall-normal and spanwise directions (Fig. 10d) are reduced in the RANS region (cf. Fig. 9d). The maximum values of the resolved turbulence and the turbulent viscosity (Figs. 10e and f) are in the fully-developed region not very different from those in Figs. 9e and

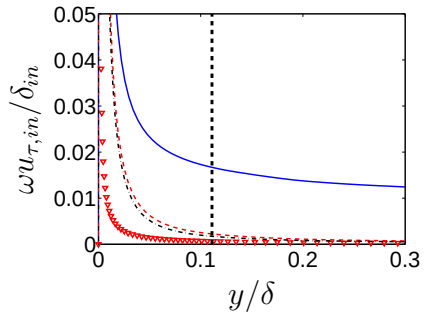

Figure 7: Boundary layer flow. $x/\delta_{in} = 0.06$. ——: $x_{tr}/\delta_{in} = 0.125$; – – –: $x_{tr}/\delta_{in} = 0.25$; –·–·–: $x_{tr}/\delta_{in} = 0.375$; ▽: at inlet (i.e. RANS). Vertical thick dashed line indicates the RANS-LES interface.

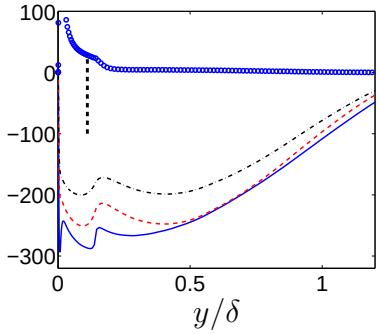

(a) $x/\delta_{in} = 0.06$. ○: Production term, $x_{tr}/\delta_{in} = 0.125$; ——: commutation term (Eq. 5), $x_{tr}/\delta_{in} = 0.125$; – – –: commutation term, $x_{tr}/\delta_{in} = 0.25$; –·–·–: commutation term, $x_{tr}/\delta_{in} = 0.375$.

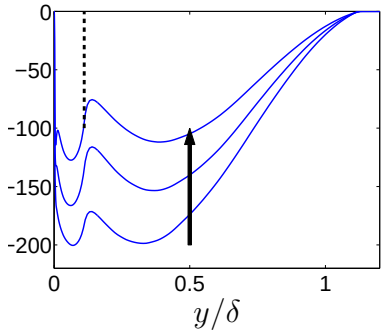

(b) Commutation term (Eq. 5). $x_{tr}/\delta_{in} = 0.375$. $x/\delta_{in} = 0.06, 0.18, 0.31$. The arrow indicates increasing x.

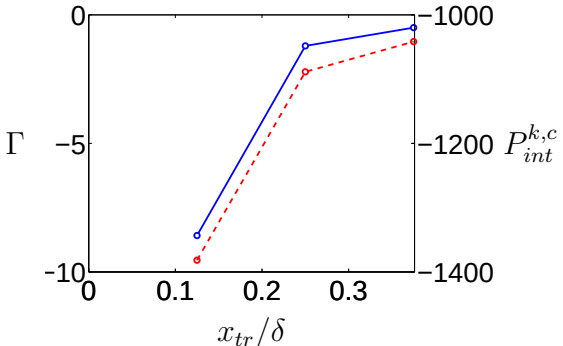

(c) Mean commutation and production terms, see Eq. 6. ——: Γ, Ratio of mean commutation term to production term (left axis); – – –: $P^{k,c}_{int}$, mean commutation term (right axis).

Figure 8: Boundary layer flow. Source terms in the k equation (scaled with $u^3_{\tau,in}/\delta_{in}$).

f, except that the maximum streamwise fluctuations are increasing all the time (Fig. 10e). The largest difference are found in the maximum turbulent viscosities for $x/\delta_{in} < 3$, cf. Figs. 9f and 10f.

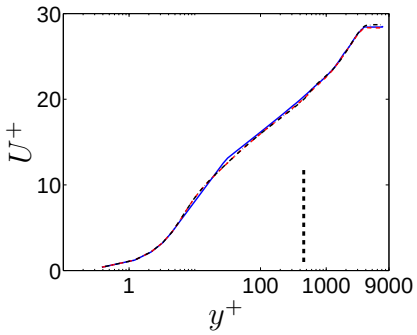

(a) Velocity. ——: inlet; – – –: $x = 2.35\delta_{in}$; –·–·–: $x = 5.95\delta_{in}$.

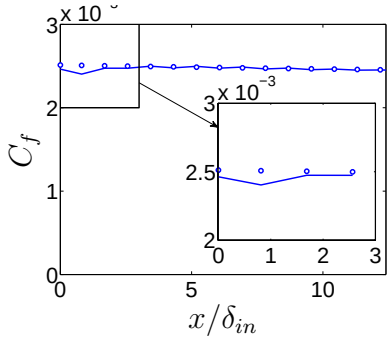

(b) skin friction. ○: $0.37\,(log_{10}Re_x)^{-2.584}$.

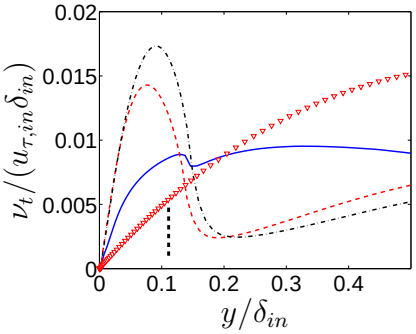

(c) Turbulent viscosity. ——: $x = 0.06\delta_{in}$; – – –: $x = 2.35\delta_{in}$; –·–·–: $x = 11.9\delta_{in}$; ▽: $\nu_t/(u_{\tau,in}\delta_{in})/80$ at inlet (i.e. RANS).

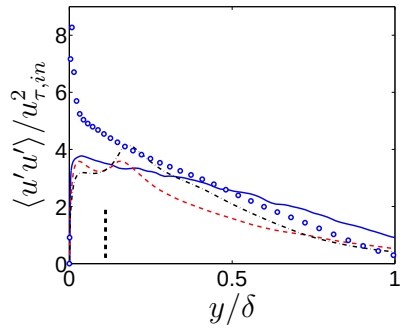

(d) Resolved turbulent fluctuations. ——: $x/\delta_{in} = 0.06$; – – –: $x = 2.35\delta_{in}$; –·–·–: $x = 11.9\delta_{in}$; ○: DNS at $Re_\theta = 8\,300$ [17].

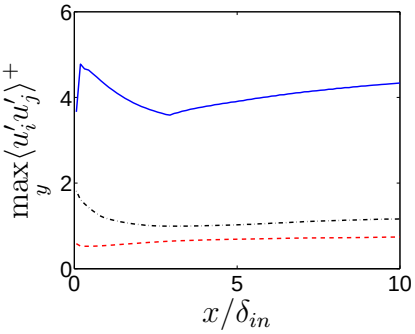

(e) Maximum resolved turbulent fluctuations. ——: $\langle u'u'\rangle^+$; – – –: $\langle v'v'\rangle^+$; –·–·–: $\langle w'w'\rangle^+$.

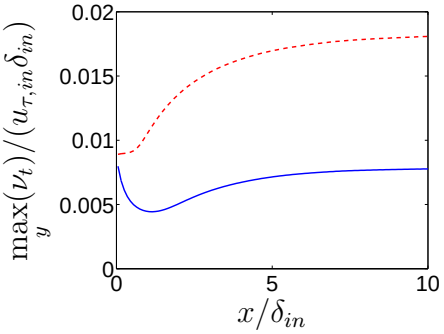

(f) Maximum turbulent viscosity. ——: LES region; – – –: RANS region.

Figure 9: Boundary layer flow. $x_{tr}/\delta_{in} = 0.125$. Vertical thick dashed line indicates the RANS-LES interface.

7. Concluding remarks

A novel method of treating k and ω at the inlet has been presented and evaluated in channel flow and boundary layer flow. A commutation term is added in the region near the inlet (i.e. the RANS-LES interface) in the k and ω equations. The commutation terms are either added only in the cells adjacent to the inlet or in a transition region; it is found that the former choice is best. For this case, this term correspond to a convection term where k is reduced from its RANS value to zero over one cell layer. The method includes no tuning constants.

It is found that the influence of the commutation terms is larger for the channel flow than for the boundary layer flow. The reason is that the importance of the commutation term in the

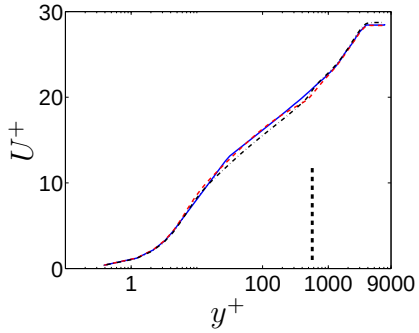

(a) Velocity. ——: inlet; – – –: $x = 2.35\delta_{in}$; –·–·–: $x = 5.95\delta_{in}$.

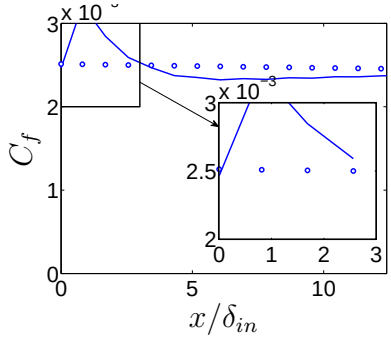

(b) skin friction. ○: $0.37\,(log_{10}Re_x)^{-2.584}$.

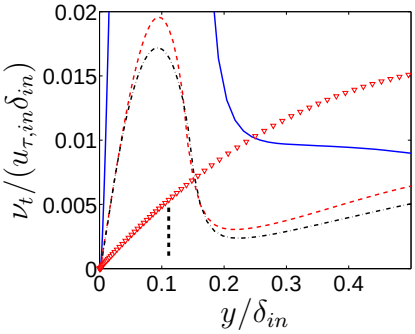

(c) Turbulent viscosity. ——: $x = 0.06\delta_{in}$; – – –: $x = 2.35\delta_{in}$; –·–·–: $x = 11.9\delta_{in}$; ▽: $\nu_t/(u_{\tau,in}\delta_{in})/80$ at inlet (i.e. RANS).

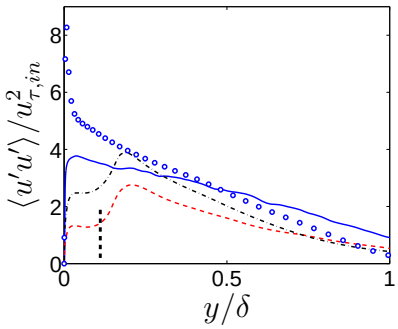

(d) Resolved turbulent fluctuations. ——: $x/\delta_{in} = 0.06$; – – –: $x = 2.35\delta_{in}$; –·–·–: $x = 11.9\delta_{in}$; ○: DNS at $Re_\theta = 8\,300$ [17].

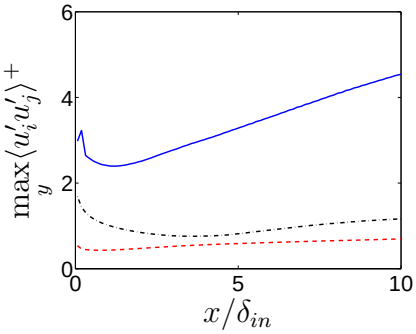

(e) Maximum resolved turbulent fluctuations. ——: $\langle u'u'\rangle^+$; – – –: $\langle v'v'\rangle^+$; –·–·–: $\langle w'w'\rangle^+$.

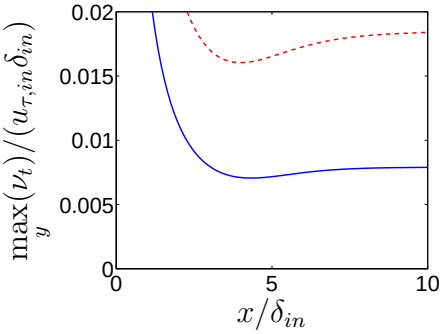

(f) Maximum turbulent viscosity. ——: LES region; – – –: RANS region.

Figure 10: Boundary layer flow. $x_{tr}/\delta_{in} = 0.125$. The commutation terms are set to zero in the RANS region. Vertical thick dashed line indicates the RANS-LES interface.

k equation compared to the production term is smaller in the boundary layer flow than in the channel flow.

References

1. F. Hamba. Analysis of filtered Navier-Stokes equation for hybrid RANS/LES simulation. *Physics of Fluids A*, 23(015108), 2011.
2. M. L. Shur, P. R. Spalart, M. Kh. Strelets, and A. K. Travin. A hybrid RANS-LES approach with delayed-DES and wall-modelled LES capabilities. *International Journal of Heat and Fluid Flow*, 29:1638–1649, 2008.

3. S. Arvidson, L. Davidson, and S.-H. Peng. Hybrid RANS-LES modeling using a low-Reynolds-number $k-\omega$ based model. In *AIAA Science and Technology Forum and Exposition, AIAA paper 2014-0225, Maryland, 13-17 January*, 2014.
4. S. Arvidson, L. Davidson, and S.-H. Peng. A hybrid RANS-LES model based on a low-Reynolds-number $k-\omega$ model (submitted). *AIAA Journal*, 2015.
5. L. Davidson and S.-H. Peng. Hybrid LES-RANS: A one-equation SGS model combined with a $k-\omega$ model for predicting recirculating flows. *International Journal for Numerical Methods in Fluids*, 43:1003–1018, 2003.
6. P. Emvin. *The Full Multigrid Method Applied to Turbulent Flow in Ventilated Enclosures Using Structured and Unstructured Grids*. PhD thesis, Dept. of Thermo and Fluid Dynamics, Chalmers University of Technology, Göteborg, 1997.
7. S. Ghosal and P. Moin. The basic equations for the large eddy simulation of turbulent flows in complex geometry. *J. Comp. Phys.*, 118:24–37, 1995.
8. S. S. Girimaji and S. Wallin. Closure modeling in bridging regions of variable-resolution (VR) turbulence computations. *Journal of Turbulence*, 14(1):72 – 98, 2013.
9. L. Davidson. A new approach to treat the RANS-LES interface in PANS. In *ETMM10: 10th International ERCOFTAC Symposium on Turbulence Modelling and Measurements*, Marbella, Spain, 2014.
10. L. Davidson. The PANS $k-\varepsilon$ model in a zonal hybrid RANS-LES formulation. *International Journal of Heat and Fluid Flow*, pages 112–126, 2014.
11. L. Davidson. Using isotropic synthetic fluctuations as inlet boundary conditions for unsteady simulations. *Advances and Applications in Fluid Mechanics*, 1(1):1–35, 2007.
12. L. Davidson and S.-H. Peng. Embedded large-eddy simulation using the partially averaged Navier-Stokes model. *AIAA Journal*, 51(5):1066–1079, 2013.
13. S-H Peng, L. Davidson, and S. Holmberg. A modified low-Reynolds-number $k-\omega$ model for recirculating flows. *Journal of Fluids Engineering*, 119:867–875, 1997.
14. S. Wallin and A. V. Johansson. A new explicit algebraic Reynolds stress model for incompressible and compressible turbulent flows. *Journal of Fluid Mechanics*, 403:89–132, 2000.
15. http://www.tfd.chalmers.se/~lada/projects/inlet-boundary-conditions/proright.html.
16. A. Lozano-Duran and J. Jimenez. Effect of the computational domain on direct simulations of turbulent channels up to $re_\tau = 4200$. *Physics of Fluids A*, 26(011702), 2014.
17. G. Eitel-Amor, R. Orlu, and P. Schlatter. Simulation and validation of a spatially evolving turbulent boundary layers up to $Re_\theta = 8300$. *International Journal of Heat and Fluid Flow*, 47:57–69, 2014.
18. M. Österlund, A.V. Johansson, H.M. Nagib, and M.H. Hites. A note on the overlap region in turbulent boundary layers. *Physics of Fluids A*, 12(1):1–4, 2000.
19. J.M. Österlund. *Experimental Studies of Zero Pressure-Gradient Turbulent Boundary-Layer Flow*. PhD thesis, Department of Mechanics, Royal Institute of Technology, Stockholm, Sweden, 1999.
20. J. O. Hinze. *Turbulence*. McGraw-Hill, New York, 2nd edition, 1975.